Nakai *et al. J Wood Sci* (2020) 66:67
https://doi.org/10.1186/s10086-020-01915-x

Journal of Wood Science

ORIGINAL ARTICLE Open Access

Flow deformation characteristics of African blackwood, *Dalbergia melanoxylon*

Kazushi Nakai[1,2*], Soichi Tanaka[2], Kozo Kanayama[2] and Tsuyoshi Yoshimura[2]

Abstract

African blackwood (ABW: *Dalbergia melanoxylon*) is a valuable tree in Tanzanian local community forests, and heartwood has been mainly utilized as an irreplaceable material in musical instruments, e.g., clarinet, oboe and piccolo. Since its use is generally for the production of musical instruments only, most of the harvested volume is wasted due to defects that would affect the quality of final products. Wood flow forming can transform bulk woods into materials in temperature/pressure-controlled mold via plastic flow deformation. The main object of this study was to evaluate the deformation characteristics of ABW heartwood in developing the potential of wasted ABW parts in terms of the effective material use. The deformation characteristics of heartwood were examined by free compression tests. Specimens were compressed along the radial direction at 120 °C, and air-dried heartwood was dramatically deformed in the tangential direction. The plastic flow deformation of ABW was amplified by the presence of both extractives and moisture. In particular, the ethanol/benzene (1:2, v/v) soluble extractives in heartwood may have contributed to flow deformation. The results of the dynamic mechanical analysis showed that the air-dried heartwood exhibited softening in a temperature range over 50 °C. The ethanol/benzene-soluble extractives contributed to the softening behavior. The clarified deformation characteristics of ABW can contribute to more efficient material use of local forests.

Keywords: *Dalbergia melanoxylon*, African blackwood, Wood flow forming, Plastic flow deformation, Dynamic viscoelasticity

Introduction

African blackwood (ABW), *Dalbergia melanoxylon*, is the national tree of Tanzania, called "Mpingo" in Swahili. The tree naturally occurs in the dryland of sub-Saharan Africa, including in eastern African countries such as Tanzania and Mozambique. These two countries actually stock intensive natural resources of this tree, and they have recently provided most ABW timber. In Tanzania, ABW trees tend to be observed in a semi-deciduous formation including deciduous and evergreen trees, i.e., the miombo woodlands, which are characterized by an abundance of three genera: *Brachystegia*, *Julbernardia* and *Isoberlinia* [1, 2]. The trees naturally grow in clusters, with a population density that has been estimated as 9–90 trees/ha [3–6].

It is mostly the heartwood of ABW that is utilized in the production of musical instruments, especially woodwinds, e.g., clarinets, oboes, piccolos, and bagpipes, due to its specific characteristics. It is normally purplish-black in color, and extremely heavy, having an air-dried density of 1.1–1.3 g/cm^3 [7, 8], while loss tangent (tanδ) in vibration properties is lower than other general hardwood species [9]. These characteristics are greatly different from those of the milky-white sapwood, which has an air-dried density of 0.75 g/cm^3 [7].

We recently reported that the growth characteristics of ABW are affected by the surrounding environment, i.e., topography, climate and human activities. Nevertheless, the tree can survive under various environmental conditions with intensive population [6]. Several defects that frequently occur in natural trees, such as lateral twists, deep fluting, and knots including

*Correspondence: kazushi.nakai@music.yamaha.com; kazushi_nakai@rish.kyoto-u.ac.jp
[2] Research Institute for Sustainable Humanosphere, Kyoto University, Gokasho, Uji, Kyoto 611-0011, Japan
Full list of author information is available at the end of the article

cracks, can affect the operation of sawmills [10]. They also influence the properties of musical instruments. Thus, sawmills can produce only a small amount of the necessary quality timber, with an actual timber yield of only 9% [11]. Currently, ABW is traded as one of the most high-priced timbers in the world; meanwhile, this inefficient utilization has threatened the species' future existence [11, 12]. In Tanzania, wasted ABW is frequently used as an energy resource, e.g., charcoal and fuelwood. As such, it is sold at prices very much lower than the timber [13]. Thus, additional uses for ABW waste could potentially contribute to the development of local communities.

Wood flow forming is a novel technique for molding three-dimensional products from bulk wood [14]. It has been suggested that wood flow deformation is plastic flow deformation due to the slipping of wood cells in or around the intercellular layers under specific temperatures [15]. Plastic flow deformation occurs under high compressive load after two types of compressive deformation stages: elastic deformation and densification deformation [15, 16]. The bulk wood of air-dried Japanese cedar (*Cryptomeria japonica*) was deformed and flowed in a mold by the addition of both high pressure and high temperature, i.e., 150 kN loading at 130 °C [17]. Furthermore, flow deformation could be promoted by increasing moisture content and/or adding thermosetting polymers [15, 17–19]. In particular, it has been suggested that an increase in the polymer content can dramatically improve flow deformation [20, 21]. Timber impregnated with polymer can flow based on the thermal softening behavior of the polymer.

The quantity of extractives in ABW heartwood has been estimated to be over 15 wt% in ethanol/benzene (1:2 v/v) solvent extraction, which is much higher than in other *Dalbergia* species, such as *Dalbergia cultrate* and *Dalbergia latifolia* [22]. The high concentrated extractives potentially work to promote flow deformation by heating beyond the thermal softening point of them. Although identification and isolation of extractives obtained from ABW heartwood have been partly reported [22–25], there is little information about the effect of extractives on the thermal behavior of ABW.

The main objective of this study was to reveal the deformation characteristics of ABW, and to discuss the relationship between flow deformation of heartwood and thermal behavior of extractives. To examine the deformation characteristics of ABW, we conducted free compression tests. In addition, the thermal behavior of extractives was evaluated based on the temperature dependence of the dynamic viscoelasticity of ABW in the modulus of transverse elasticity. We mainly focused on the heartwood which occupies the large part of ABW trees, so that the results might contribute to improvement of the general material utilization of ABW.

Materials and methods

Wood specimens

Specimens of ABW were obtained from logs over 24 cm in diameter at breast height, harvested in 2018 at the Forest Stewardship Council (FSC)-certified forest located in the Kilwa District, Lindi Region, Tanzania. Two types of specimens were prepared for this study. Disk-shaped specimens of ABW heartwood obtained from tangential sections of the wood with 15-mm diameter (longitudinal, $L \times$ tangential, T) and 2-mm thick in the radial direction were prepared for the free compression test with 20 replicates. Rectangular specimens of ABW (heartwood and sapwood), measuring 30 mm (L; longitudinal direction) $\times$ 1 mm (R; radial direction) $\times$ 5 mm (T; tangential direction), were prepared for the dynamic mechanical analysis with 15 replicates per specimen. All specimens were cut from air-dried timber conditioned for over 3 months at room temperature, and specimens were kept in a controlled chamber (KCL-2000, Tokyo Rikakikai Co. Ltd., Tokyo, Japan) conditioned at 22 ± 2 °C and 60% relative humidity (RH) for over 30 days.

Pretreatment prior to the tests

Figure 1a, b shows the experimental procedures for the disk-shaped and rectangular specimens, respectively. For both, four types of treatment [air-drying (AD), water extraction (WT), ethanol/benzene extraction (EB), and oven-drying (OD)], were prepared with 5 replicates according to the experimental procedures (Fig. 1a, b). All specimens were oven-dried at 105 °C for over 24 h, and their oven-dried weights (W_0) were measured with an electronic scale (GH-252, A&D Company Ltd., Tokyo, Japan).

The extraction processes were applied for the WT and EB specimens (Fig. 1). Water extraction was performed as follows. Oven-dried specimens were soaked in 150 mL of distilled water using a sealed Erlenmeyer flask. The soaked specimens were stirred for 10 min in the water bath at 40 °C with ultrasonic treatment (Branson 5510JDTH, Yamato Scientific Co., Ltd., Tokyo, Japan), and then kept in the controlled chamber at 45 ± 5 °C for 48 h. For the extraction, specimens from different sampling parts (heartwood, sapwood) were placed in different flasks to prevent the migration of extractives between parts. For the EB specimens, extraction was performed in the same way using an (1:2, v/v) ethanol/benzene solution instead of water.

After extraction, both the WT and EB specimens were stored at room temperature for over 1 week, and then oven-dried at 105 °C for over 24 h to measure the extracted

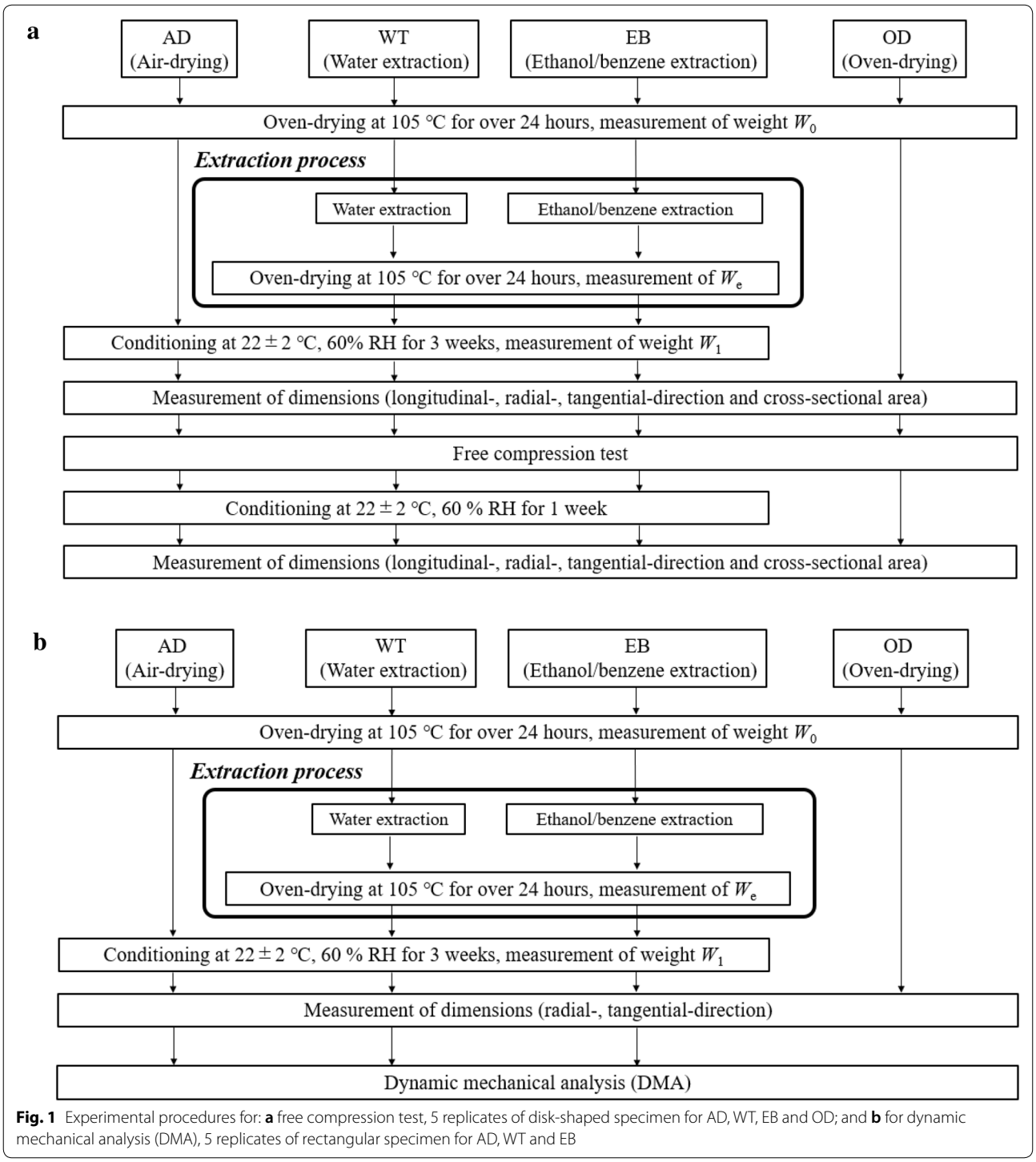

Fig. 1 Experimental procedures for: **a** free compression test, 5 replicates of disk-shaped specimen for AD, WT, EB and OD; and **b** for dynamic mechanical analysis (DMA), 5 replicates of rectangular specimen for AD, WT and EB

weight (W_e) with the electric scale (Fig. 1a, b). The extraction rate was calculated by Eq. 1 using W_0 and W_e:

$$\text{Extraction rate} = \frac{W_0 - W_e}{W_0} \times 100(\%). \quad (1)$$

The AD and extracted WT and EB specimens were conditioned at 22 ± 2 °C and 60% RH for over 3 weeks. The conditioned weight (W_1) was then measured with the electric scale. In addition, the dimensions of each specimen were measured after the conditioning process, as described later. The moisture content (MC) of each

specimen was calculated before the tests using the following Eqs. 2a and 2b:

$$\mathrm{MC} = \frac{W_1 - W_0}{W_0} \times 100(\%), \tag{2a}$$

$$\mathrm{MC} = \frac{W_1 - W_e}{W_e} \times 100(\%). \tag{2b}$$

The MC of AD specimens was calculated using Eq. 2a, while that of extracted specimens (WT and EB) was calculated using Eq. 2b.

The dimensions of AD, WT, EB, and OD specimen were measured just before the tests (Fig. 1a, b). For the specimens provided to free compression test (Fig. 1a), the dimension of radial direction (*R*-direction, h_0) was measured at the center point of specimens with a micrometer (OMV-25MX, Mitutoyo Corp., Kawasaki, Japan); the dimensions of longitudinal (*L*-direction) and tangential directions (*T*-direction) were measured at the centerline of each direction with a digital caliper (CD-15CP, Mitutoyo Corp., Kawasaki, Japan). The cross-sectional area was calculated using the image processing software ImageJ [26, 27]. For dynamic mechanical analysis (DMA) specimens (Fig. 1b), *R*-direction and *T*-direction dimensions were measured at the centerline of each with the above-noted digital caliper.

Free compression test

The free compression test was performed with a universal testing machine (Instron 5582, Instron Co., MA, USA) as illustrated in Fig. 2. Specimens were placed on the lower punch controlled at 120 °C, and held in place with the upper punch without loading for the pre-heating time of 60 s. (Fig. 2). They were then compressed at a constant speed (0.02 mm/s), while both compressive stress (*P*) and gap displacement caused by deformation of specimen (h_s) were measured. Compression was also performed without specimens, the *P* and the gap displacement caused by deformation of punches (h_b) were measured. The actual displacement (h) was calculated using Eq. 3:

$$h = h_s + h_b. \tag{3}$$

The stress–strain curve was described using nominal strain (ε) and nominal stress (σ) calculated using Eqs. 4 and 5:

$$\varepsilon = 1 - (h/h_0), \tag{4}$$

$$\sigma = P/(\pi d^2/4), \tag{5}$$

where h_0 is the initial specimen thickness (in the *R*-direction), π is the circular constant, and d is the diameter of the punch ($d = 15$ mm). Specimens were compressed to a maximum compressive load of 20 kN, equivalent to 113 MPa in compressive stress. In this study, water vapor pressure, caused by heating air-dried specimens, was neglected due to the small specimen size.

After the test, all specimens except for the OD were placed in a controlled chamber for 1 week at 22 ± 2 °C and 60% RH for conditioning, and the parameters of specimen weight, dimensions (*L*-direction, *R*-direction, and *T*-direction) and cross-sectional area, were measured (Fig. 1a). The parameters of OD were measured immediately after the test. Dimensional changes (D_c) caused by the test (*L*-direction, *T*-direction and cross-sectional area) were calculated by Eq. 6:

$$D_c = \frac{D_a - D_b}{D_b} \times 100(\%), \tag{6}$$

where D_b and D_a are the dimensional values of specimens before and after the test, respectively.

The physical parameters, Young's modulus and maximum strain, were determined from the stress–strain curve collected through the test results. Young's modulus (E) was calculated from the angle of elastic deformation area in the curve. The stress at the flow-starting point (σ_f) was defined as the inflexion point of the stress–strain curve (Fig. 3), where the first peak of the derivative stress with respect to the strain ($d\sigma/d\varepsilon$). The strain at the inflection point was defined as the flow-starting strain (ε_f). The maximum strain (ε_m) was defined as the compressive strain value at the maximum compressive stress, $\sigma_m = 113$ MPa in the test.

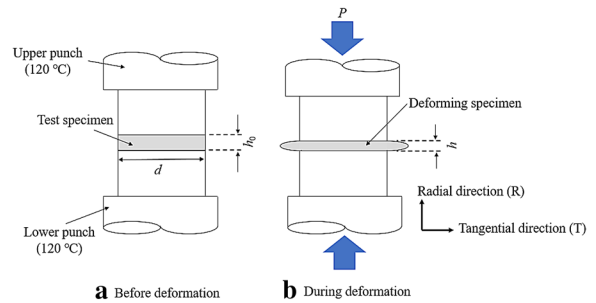

Fig. 2 Schematic diagram of free compression test. *d*: specimen diameter, h_0: initial thickness, *h*: deformed thickness

Dynamic mechanical analysis

The DMA was performed using a rheometer (ARES-G2, TA Instruments, New Castle, USA). The complex dynamic modulus (G^*) of viscoelastic materials generally represents the relation between the storage modulus (G') and loss modulus (G''), which are calculated from the

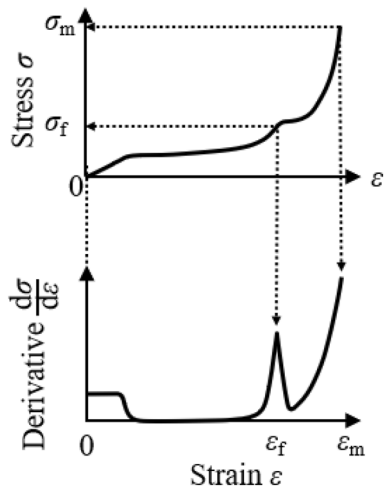

Fig. 3 Method for calculating the deformation parameters from the stress–strain curve

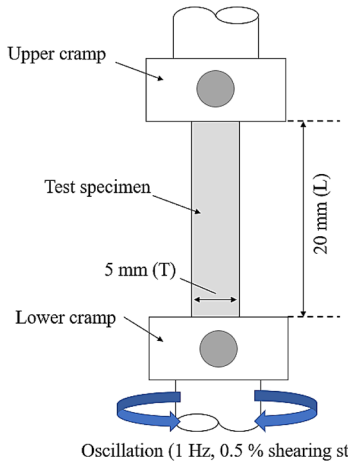

Fig. 4 Experimental set-up for the dynamic mechanical analysis using a rheometer

dynamic performance with oscillation stress and strain by Eqs. 7 and 8:

$$G^* = G'(\omega) + iG''(\omega) = |G^*|(\cos\delta + i\sin\delta), \quad (7)$$

$$\tan\delta = G''(\omega)/G'(\omega), \quad (8)$$

where i is the imaginary number, ω is the angular frequency, δ is the phase angle, and tanδ is the loss factor. In this study, G', G'' and tanδ were calculated from the amplitude and phase difference (δ) of the oscillation curve for torque using the analysis software (TRIOS, TA Instruments, New Castle, USA).

The temperature-ramp test was conducted under a controlled environment by N_2 purge, from − 50 to 250 °C at a constant temperature ramp rate (5 °C/min). Both edges of specimens were cramped at 20 mm in the *L*-direction, and loaded with dynamic torsion, 0.5% oscillation shearing strain at a constant frequency of 1.0 Hz (Fig. 4).

Statistical analysis

The Tukey–Kramer test at 1% critical difference ($p < 0.01$) was used to analyze statistical differences between values (BellCurve for Excel, Social Survey Research Information Co. Ltd., Tokyo, Japan).

Results and discussion

Deformation characteristics

In the free compression test, both AD and WT specimens were flowed in the *T*-direction at 120 °C, while EB and OD specimens were not flowed (Figs. 5, 6). These findings suggest it was possible that flow deformation was promoted by the extractives and moisture.

In this study, AD showed the largest flow deformation compared to the other specimens. Table 1 lists the extraction rate, initial MC, and dimensional change for both the *L*- and *T*-directions together with specimens' cross-sections. In the cross-sectional area, AD was again the highest (average ca. 117%) of all specimens with a significant difference at 1% level. For AD, the dimensional change in the *T*-direction was also the highest among specimens, whereas those in *L*-direction had no significant difference. These dimensional values in the vertical direction of compression loading show the displacement caused by flow deformation. The results suggest that the changes in the *T*-direction corresponded strongly to flow deformation based on the wood anisotropy: the lower strength on *T*-direction than *L*-direction. Yamashita et al. [17] found that flow direction was mainly perpendicular to the fiber orientation, which was in keeping with our findings.

Figure 7a, b shows the σ_f and ε_f values for each specimen, the stress and strain values specialized at the flow-starting point. The σ_f value indicates the stress value necessary to generate flow deformation. AD showed the lowest value (average ca. 33.0 MPa) of all specimens, while WT, EB and OD values were significantly higher (Fig. 7a). The ε_f value indicates the strain required to initiate flow deformation. There was a significant difference between the non-extracted specimens (AD and OD) and the extracted specimens (WT and EB) at 1% level (Fig. 7b).

Figure 8 shows the maximum strain (ε_m) values. The ε_m value reflects the total displacement by the loaded compressive stress, i.e., elastic deformation, densification

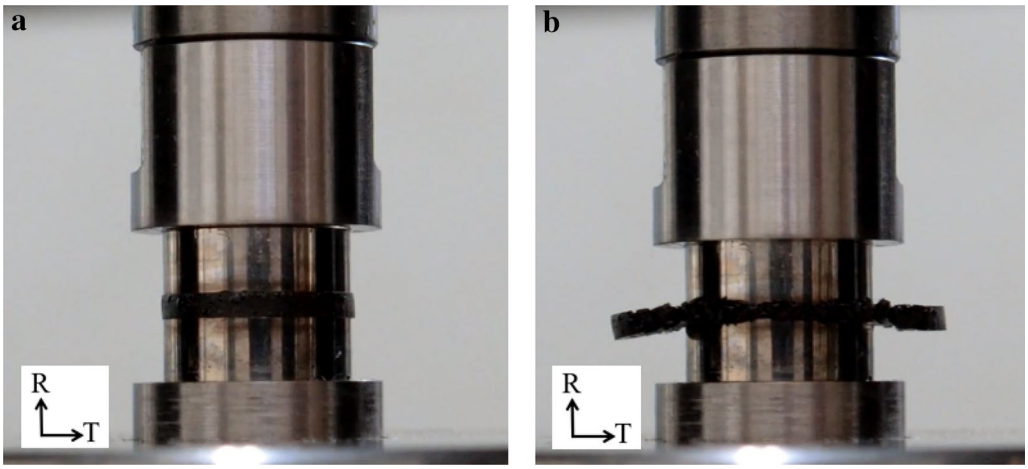

Fig. 5 Specimen in the free compression test: **a** before and **b** after compression up to 113 MPa compressive stress

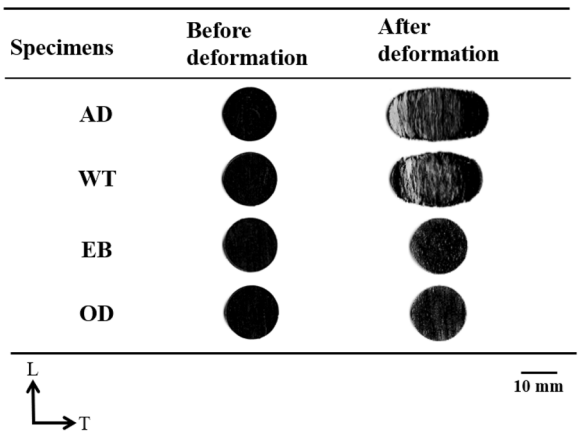

Fig. 6 Representative change in shapes of specimens before and after the free compression test

deformation, and flow deformation. Here, there were significant differences among all specimens at 1% level: ca. 73% (AD), ca. 58% (WT), ca. 28% (EB) and ca. 10% (OD) on average. The difference in the strain between ε_m and ε_f ($\Delta\varepsilon = \varepsilon_m - \varepsilon_f$), which indicated the displacement due to flow deformation, showed a significantly high value in AD (ca. 58.4%) at 1% level (Figs. 7b, 8). Although there was no statistical difference among the values of other specimens, the variation depended on extractives and moisture: ca. 21.2% (WT), ca. 0.80% (EB) and ca. 1.30% (OD) (Figs. 7b, 8). Therefore, it was suggested that extractives and moisture amplified flow deformation.

The ethanol/benzene extractives appeared to influence the deformation characteristics. Young's modulus (E) of specimens is shown in Fig. 9. The E values of WT and EB were statistically similar to that of AD at the 1% level, despite their average values being more than 2 times higher: 300.9 MPa (AD), 641.5 MPa (WT) and 999.6 MPa (EB). The MC of EB was also similar to those of AD and WT (Table 1). This suggested that the ethanol/benzene-soluble extractives likely increased the elastic deformation of ABW. The σ_f value in EB was the highest among all specimens, although statistically equal to OD (Fig. 7a). The ε_f value in EB was higher than AD (Fig. 7b), although the ε_m value in EB was significantly lower than WT and AD with only 1% of dimensional change (Table 1, Fig. 8). The value of $\Delta\varepsilon$ in EB was also significantly lower than AD (Figs. 7b, 8). These findings suggested that the

Table 1 Extraction rate, moisture content (MC) and dimensional changes due to free compression (mean ± SD)

Specimens	Extraction rate %*	Moisture content %*	Dimensional change %		
			Cross-sectional area*	*L*-direction*	*T*-direction*
AD		8.24 ± 0.61[a]	117.39 ± 7.90[c]	−0.52 ± 1.21[a]	97.45 ± 10.00[c]
WT	1.89 ± 0.44[a]	8.88 ± 1.22[a]	83.02 ± 3.38[b]	3.54 ± 4.54[a]	66.06 ± 24.24[b]
EB	16.12 ± 1.23[b]	8.69 ± 0.11[a]	1.01 ± 1.20[a]	−0.51 ± 1.46[a]	1.13 ± 0.63[a]
OD			1.15 ± 0.86[a]	0.61 ± 0.55[a]	2.29 ± 0.85[a]

* Means with the same letter (a, b, c) are not significantly different (Tukey–Kramer test, $p < 0.01$) ($n = 5$)

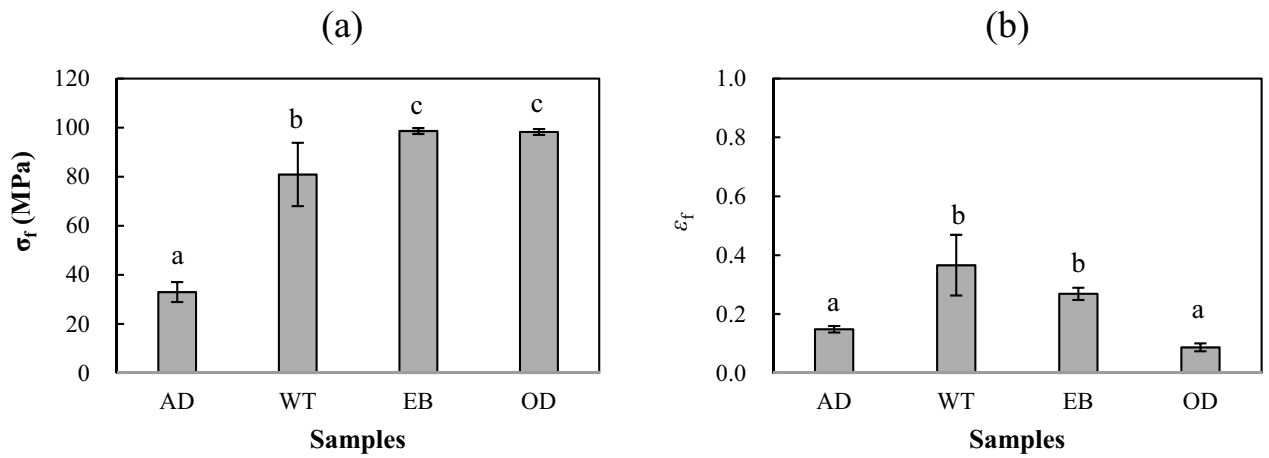

Fig. 7 Stress and strain at flow-starting point. **a** Compressive stress at the flow-starting point (σ_f). **b** Compressive strain at the flow-starting point (ε_f). Means with the same letter (a, b, c) are not significantly different (Tukey–Kramer test, $p < 0.01$) ($n = 5$). Error bars represent standard deviations

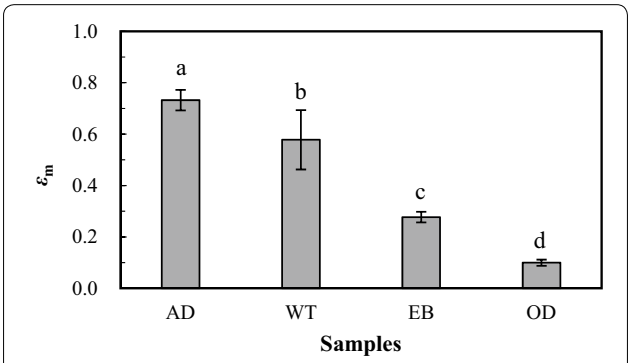

Fig. 8 Maximum strain at the maximum load (ε_m). Means with the same letter (a, b, c, d) are not significantly different (Tukey–Kramer test, $p < 0.01$) ($n = 5$). Error bars represent standard deviations

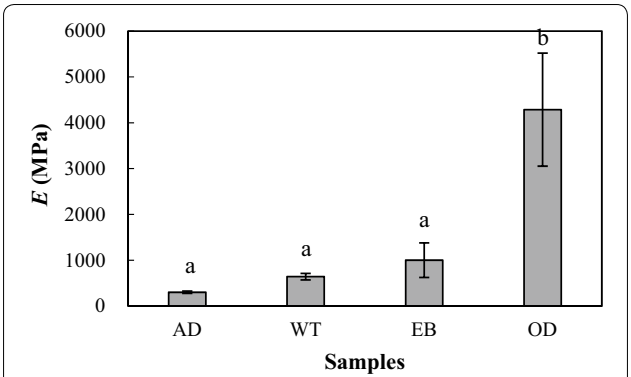

Fig. 9 Young's modulus (E) of specimens in the compressive fluidity tests. Means with the same letter (a, b) are not significantly different (Tukey–Kramer test, $p < 0.01$) ($n = 5$). Error bars represent standard deviations

ethanol/benzene-soluble extractives helped promote the flow deformation of ABW.

The significant improvement of wood plastic deformation by increasing resin content has been reported previously [19–21, 28]. Wood extractives are generally distributed in cell walls and intercellular layers, as well as in lumen. Therefore, the presence of extractives potentially influences plastic deformation, despite their small amounts. In this study, EB showed a significantly higher extraction rate than WT: 16.12% (EB) and 1.89% (WT) on average (Table 1). The ethanol/benzene-soluble extractives comprising over 16 wt% of ABW heartwood (Table 1) [22], apparently have a large impact on ABW deformation characteristics.

The water-soluble extractives might also influence deformation characteristics. Dimensional change in the cross section of WT was significantly lower than that of AD: average ca. 83% (Table 1). The σ_f value in WT was higher than AD at 1% level: average ca. 80.9 MPa (Fig. 7a). The value of $\Delta\varepsilon$ in WT was also significantly lower, as previously noted. Furthermore, an increase of E in WT was observed though the value was not statistically different from AD (Fig. 9). Therefore, the presence of water-soluble extractives also contributed to promoting the flow deformation of ABW. These results might also indicate a positive relationship between water-soluble extractives and the deformation loading required to generate flow deformation.

The moisture in wood also affected the deformation characteristics. As shown in Table 1, flow deformation was not observed in OD, even though extractives were present. The σ_f value in OD was approximately three times higher than in AD (Fig. 7a), and $\Delta\varepsilon$ values were also

lower than AD (Figs. 7b, 8). Furthermore, the *E* value of OD was markedly higher than the others (Fig. 9). This suggested that the deformation characteristics of ABW heartwood were affected by moisture. The moisture content influenced the elastic deformation of ABW, and possibly amplified even plastic deformation. Previous reports also noted that moisture contributed to wood-softening behavior, and that wood flow deformation could be improved in proportion to the increase in MC [17, 21]. It is possible that the lower value of *E* contributed to densification deformation and flow deformation, while the change in *E* depended on the moisture content of specimens.

Temperature dependence of dynamic viscoelasticity

Table 2 presents the extraction rate and MC of specimens used for the DMA. The EB-heartwood had a significantly high extraction rate (average ca. 11.3%) compared to other specimens, including the EB-sapwood (average ca. 2.4%). By contrast, the rates in the WT-heartwood and sapwoods were similar. Therefore, the ethanol/benzene-soluble extractives were definitely concentrated in the heartwood. Meanwhile, the MCs of heartwoods (8–9%) were a bit lower than those of sapwoods (9–11%), and the extractions showed no effect. The MC of EB-sapwood was statistically equal to that of heartwood, which was significantly lower than the other sapwood specimens. Extractives have been suggested to affect the sorption properties of wood [29–31], and the removal of extractives could result in an increase in swelling–shrinkage behavior [32–34]. Water-soluble extractives have been reported not to affect the wood sorption properties [34, 35]. Our results did not show any clear effects of the extractives on the sorption properties of ABW.

Figure 10 shows the temperature dependence of the dynamic viscoelastic parameters of AD, WT and EB specimens. The curves of heartwood specimens were obviously shifted toward flattened curves in a range over 50 °C due to the extractions, whereas the curves of sapwoods were not shifted. Amorphous polymers such as lignin and hemicellulose generally influence the temperature dependence of dynamic viscoelasticity in wood, with variable performance related to MC [36–38]. In this study, the modulus of transverse elasticity obtained by the DMA depended on the extractives, and were relevant to the flow deformation characteristics.

Table 2 Extraction rate and MC of specimens in the dynamic mechanical analysis (mean ± SD)

Specimen	Extraction rate %*		Moisture content %*	
	Heartwood	Sapwood	Heartwood	Sapwood
AD			8.01 ± 0.73^{a}	10.83 ± 0.76^{b}
WT	2.17 ± 0.78^{a}	3.67 ± 1.34^{a}	8.83 ± 0.84^{a}	10.52 ± 0.59^{b}
EB	11.32 ± 3.54^{b}	2.36 ± 1.24^{a}	8.72 ± 0.50^{a}	9.13 ± 0.64^{a}

* Means with the same letter (a, b) are not significantly different (Tukey–Kramer test, $p < 0.01$) ($n = 5$)

The G' values of all heartwood specimens overlapped from 120–130 to 250 °C (Fig. 10a). From − 50 to 120–130 °C, AD, WT and EB-heartwood specimens showed a similar pattern of curves, with a sharp decrease after 50 °C. The values were highest in AD specimens, followed by WT, and the lowest in EB specimens. By contrast, all G' curves overlapped from – 50 to 250 °C in the sapwood specimens. Different trends of G' curves were found between heartwood and sapwood in the range of 50 °C to 120–130 °C. Multiple inflection points could be clearly observed in the AD-heartwood specimens, but the AD-sapwood specimens exhibited a single inflection point in this range.

The increase in G'' and tanδ generally indicates an increase in the viscosity of a material, which might be related to deformation characteristics. Since we noted the large flow deformation in the AD-heartwood, our results suggested that the patterns of G'' and tanδ curves are correlated with flow deformation in regard to the extractives, as discussed above (Figs. 6, 7, 8a, Table 1). The G'' curves showed that the AD-heartwood had multiple shoulder peaks, and higher peak values in the range of 50–150 °C, suggesting that the viscosity of AD-heartwood was also increased, because the rapid increase of tanδ was simultaneously observed in this range (Fig. 10a). Although the similar patterns were observed in the curves of WT- and EB-heartwood, the values were decreased by the extraction. The G'' value of EB-heartwood was the lowest of all the heartwoods, and its shifted curve almost overlapped that of sapwood specimens (Fig. 10a, b). The curves of sapwood specimens did not shift through the extractions with lower values in the range. As a result, sapwood might not show flow deformation like EB-heartwood in the free compression test. In addition, the potential of flow deformation under other temperatures was also assumed based on the curves of G'' and tanδ. The flow deformation of ABW heartwood was observed at 120 °C in this study (Figs. 5, 6). The results in Fig. 10a suggest that the AD-heartwood potentially flowed under temperatures lower than 120 °C due to the significant increase in G'' and tanδ in the range over 50 °C. Lower temperature should be useful not only for preserving the original mechanical properties, but also for controlling viscosity in the mold.

Extractives were suggested to affect the softening temperature of the wood, which has particularly large amounts of ethanol/benzene extractives, like those reported in pao rosa (*Swartzia fistuloides*) [39]. The sharp increases of G'' and tanδ in the AD-heartwood

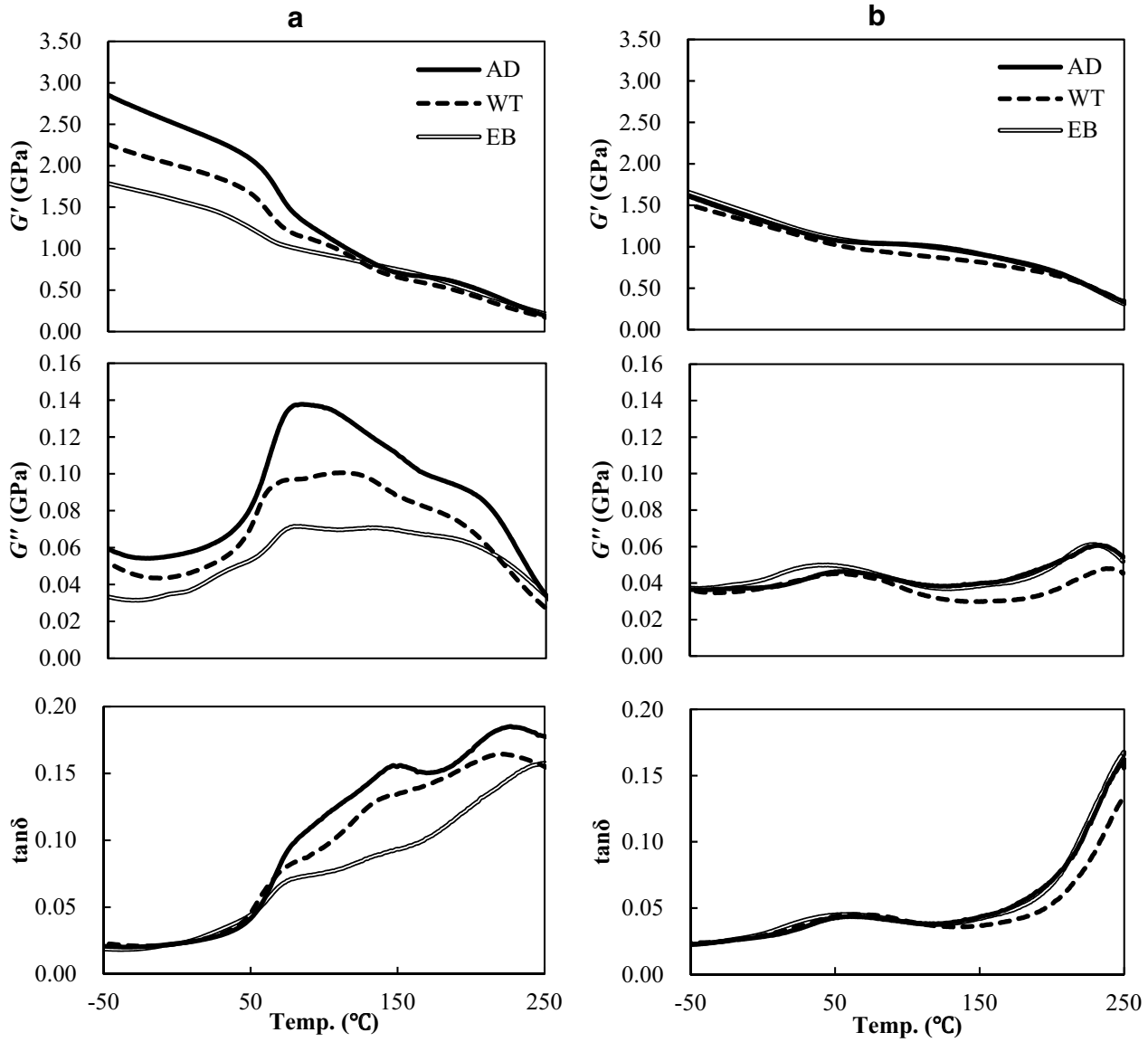

Fig. 10 Temperature dependence of the dynamic viscoelasticity among extraction treatments in **a** heartwood and **b** sapwood specimens

at 50–80 ℃ may indicate the softening behavior of extractives. The lowest values of both *G″* and tan*δ* were observed in the EB-heartwood (Fig. 10a). Although all the tan*δ* curves of heartwoods were essentially overlapped in the range under 50 °C, the sharp increase of tan*δ* showed a significant increase of *G″* in this range. This suggested the ethanol/benzene-soluble extractives were softened in the range over 50 °C. The curves of WT-heartwood also suggested that the water-soluble extractives affected the dynamic viscoelasticity of AD-heartwood (Fig. 10a). The water extraction resulted in ca. 30% reduction in the *G″* value of WT-heartwood at 120 ℃, and the static parameters of WT-heartwood were statistically different from those of AD-heartwood (Figs. 7, 8). This trend was observed only in the heartwood specimens, even though the extraction rate in WT-sapwood was same as the WT-heartwood (Table 2). Although further studies are needed to identify the effect of water-soluble extractives, we assumed that some extractives were duplicated by the ethanol/benzene extraction due to the similarity of solubility parameters between ethanol and water [40].

Conclusions

The application of wood flow forming techniques in ABW could contribute to developing the effective utilization of wasted ABW timbers in the local forest sector. The present study demonstrated the deformation characteristics of air-dried ABW heartwood via the free compression test. The air-dried heartwood of ABW flowed at 120 ℃, our findings suggested that the extractives in heartwood definitely resulted in flow deformation. The flow deformation depended mainly on the ethanol/benzene-soluble extractives, which were highly concentrated in the heartwood. The ethanol/benzene-soluble extractives were suggested to be softened at temperatures over 50 ℃. The DMA results indicated that the increase in G'' and tanδ were strongly related to flow deformation in the free compression test; thus, the potential of flow formation at other temperatures was also assumed in the DMA. The flow deformation of ABW also depended on MC, although the oven-dried heartwood did not flow even with the presence of extractives. The MC affected mechanical properties, and an increase in MC might result in flow deformation. Consequently, our findings suggest the possibility that wood flow forming might contribute to further utilization of ABW timbers wasted in local sawmill factories.

Abbreviations

ABW: African blackwood; tanδ: Loss tangent in vibration properties; FSC: Forest Stewardship Council; AD: Air-drying; WT: Water extraction; EB: Ethanol/benzene extraction; OD: Oven-drying; RH: Relative humidity; W_0: Oven-dried weight; W_e: Extracted weight; W_1: Conditioned weight; MC: Moisture content; *R*: Radial; *L*: Longitudinal; *T*: Tangential; *P*: Compressive stress; h_s: Gap displacement caused by deformation of specimen; h_b: Gap displacement caused by deformation of punches; *h*: Actual displacement; ε: Nominal strain; σ: Nominal stress; h_0: Initial thickness of specimen; π: The circular constant; *d*: Diameter of punch; DMA: Dynamic mechanical analysis; D_c: Dimensional change; D_a: Dimensional value before free compression test; D_b: Dimensional value after free compression test; *E*: Young's modulus; σ_f: Stress at the flow-starting point; dσ/dε: Derivative stress with respect to strain; ε_f: Flow-starting strain; ε_m: Maximum strain; σ_m: Maximum compressive stress; G^*: Complex dynamic stress; G': Storage modulus; G'': Loss modulus; *i*: The imaginary number; ω: Angular frequency; δ: Phase angle.

Acknowledgements

A part of this article was presented at 2018 SWST/JWRS International Convention, Nagoya, Japan, November 2018, and at the 70th Annual Meeting of the Japan Wood Research Society, Tottori, Japan, March 2020. We thank Akio Adachi, Research Institute for Sustainable Humanosphere, Kyoto University, for his help in preparing test specimens. We also thank Makala Jasper and Jonas Timothy, Mpingo Conservation & Development Initiative, Tanzania, for their kind assistance in helping us understand local forests. We would like to express our gratitude to Neil Bridgland and James Laizer, Sound & Fair Ltd., in Tanzania, and Motoki Takata and Shoko Ishii, Yamaha Corporation for collecting wood samples. Our appreciation also goes out to all the Tanzanian local villagers for their kind support.

Authors' contributions

KN designed the study, prepared wood samples, analyzed data and wrote the manuscript. ST and KK assisted in data collection and contributed to interpretation. ST, KK and TY critically reviewed the manuscript. All authors read and approved the final manuscript.

Funding

This work was supported as a part of a joint study for fundamental research on achieving sustainable forest utilization focusing on African blackwood (*Dalbergia melanoxylon*) by the Yamaha Corporation, Research Institute for Sustainable Humanosphere, Kyoto University and the Graduate School of Agriculture, Kyoto University.

Availability of data and materials

The datasets used and/or analyzed during the current study are available from the corresponding author on reasonable request.

Competing interests

The authors declare that they have no conflict of interest.

Author details

[1] Musical Instruments & Audio Products Production Unit, Yamaha Corporation, 10-1 Nakazawa-cho, Naka-ku, Hamamatsu 430-8650, Japan. [2] Research Institute for Sustainable Humanosphere, Kyoto University, Gokasho, Uji, Kyoto 611-0011, Japan.

Received: 18 June 2020 Accepted: 14 September 2020
Published online: 29 September 2020

References

1. Campbell B, Frost P, Byron N (1996) Miombo woodlands and their use: overview and key issues. In: Campbell B (ed) The miombo in transition: woodlands and welfare in Africa. Center for International Forestry Research (CIFOR), Bogor, pp 1–10
2. White F (1983) The Zambezian regional centre of endemism. In: White F (ed) The vegetation of Africa: a descriptive memoir to accompany the UNESCO/AETFAT/UNSO vegetation map of Africa (Natural Resources Research 20). UNESCO, Paris, pp 86–101
3. Gregory A, Ball SMJ, Eziefula UE (1999) Tanzanian Mpingo 98 full report. Mpingo Conservation Project, Tanzania
4. Opulukwa MJ, Hamza KFS, Malende YHMB (2002) Inventory of *Dalbegia melanoxylon* (Mpingo) in the southern part of Tanzania: the case of Nachingwea. Afr Study Mono 23(1):1–10
5. Mariki AS, Wills AR (2014) Environmental factors affecting timber quality of African Blackwood (Dalbergia melanoxylon). Mpingo Conservation & Development Initiative, Kilwa Masoko
6. Nakai K, Ishizuka M, Ohta S, Timothy J, Jasper M, Lyatura NM, Shau V, Yoshimura T (2019) Environmental factors and wood qualities of African blackwood, *Dalbergia melanoxylon*, in Tanzanian Miombo natural forest. J Wood Sci 65(1):39
7. Malimbwi RE, Luoga EJ (2000) Prevalence and standing volume of *Dalbergia melanoxylon* in coastal and inland sites of southern Tanzania. J Tropical For Sci 12(2):336–347
8. Sproßmann R, Zauer M, Wagenfur A (2017) Characterization of acoustic and mechanical properties of common tropical woods used in classical guitars. Res Phys 7:1737–1742
9. Brémaud I, El Kaïm Y, Guibal D, Minato K, Thibaut B, Gril J (2012) Characterisation and categorisation of the diversity in viscoelastic vibrational properties between 98 wood types. Ann For Sci 69(3):373–386
10. Lovett J (1987) Mpingo—the African blackwood. Swara 10:27–28
11. Jenkins M, Oldfield S, Aylett T (2002) International trade in African blackwood. Fauna & Flora International, Cambridge
12. Hamisy WC, Hantula J (2002) Characterization of genetic variation in African Blackwood, *Dalbergia melanoxylon* using random amplified microsatellite (RAMS) method. Plant genetic resources and biotechnology in Tanzania, part 1: biotechnology and social aspects. In: Proceedings of the second national workshop on plant genetic resources and biotechnology, Arusha, Tanzania, 6–10 May 2002
13. Miya M, Ball SMJ, Nelson FD (2012) Drivers of deforestation and forest degradation in Kilwa District. Mpingo Conservation & Development Initiative, Kilwa
14. Yamashita O, Yokochi H, Miki T, Kanayama K (2007) Producing cups from wood by extrusion using flow phenomenon of bulk wood. Nihon Kikai Ronbun 73(729):2074–2078 **(in Japanese)**

15. Miki T, Sugimoto H, Shigematsu I, Kanayama K (2014) Superplastic deformation of solid wood by slipping cells at sub-micrometre intercellular layers. Int J Nanotechnol 11(5–8):509–519
16. Sugino H, Tanaka S, Kasamatsu Y, Okubayashi S, Seki M, Miki T, Umemura K, Kanayama K (2020) Influence of electron-beam irradiation on plastic flow deformation of wood. J J Wood Res Soc 66(2):59–66 **(in Japanese)**
17. Yamashita O, Yokochi H, Miki T, Kanayama K (2009) The pliability of wood and its application to molding. J Mater Proc Technol 209:5239–5244
18. Miki T, Seki M, Sugimoto H, Shigematsu I, Kanayama K (2013) Preparation of three dimensional products using flow deformability of wood treated by small molecular resins. Adv Mater Res 856:79–86
19. Seki M, Tanaka S, Miki T, Shigematsu I, Kanayama K (2017) Forward extrusion of bulk wood containing polymethylmethacrylate: effect of polymer content and die angle on the flow characteristics. J Mater Proc Technol 239:140–146
20. Seki M, Tanaka S, Miki T, Shigematsu I, Kanayama K (2016) Extrudability of solid wood by acetylation and in-situ polymerization of methyl methacrylate. BioResources 11(2):4205–4036
21. Seki M, Kiryu T, Miki T, Tanaka S, Shigematsu I, Kanayama K (2016) Extrusion of solid wood impregnated with phenol formaldehyde (PF) resin: effect of resin content and moisture content on extrudability and mechanical properties of extrudate. BioResources 11(3):7697–7709
22. Yin X, Huang A, Zhang S, Liu R, Ma F (2018) Identification of three *Dalbergia* species based on differences in extractive components. Molecules 23(9):1–11
23. Eyton WB, Ollis WD, Sutherland IO (1967) The neoflavanoids group of natural products-I: Dalbergiones a new class of quinones. Tetrahedron 21(9):2683–2696
24. Donnelly BJ, Donnelly DMX, O'Sullivan AM, Predergast JP (1969) Dalbergia species VII, isolation and structure of melanoxin a new dihydrobenzofuran from *Dalbergia melanoxylon* Guill. and Perr. (Leguminoseae). Tetrahedron 25(18):4409–4414
25. Seshadri TR (1972) Polyphenols of *Pterocarpus* and *Dalbergia* woods. Phytochemistry 11(3):881–898
26. Rasband WS (1997–2012) ImageJ, U. S. National Institutes of Health, Bethesda, Maryland, USA. https://rsb.info.nih.gov/ij/. Accessed 12 Mar 2020
27. Schneider CA, Rasband WS, Eliceiri KW (2012) NIH Image to ImageJ: 25 years of image analysis. Nat Methods 9:671–675
28. Shams MI, Yano H, Endou K (2006) Compressive deformation of wood impregnated with low molecular weight phenol formaldehyde (PF) resin I: effects of pressing pressure and pressure holding. J Wood Sci 50:337–342
29. Nzokou P, Kamdem DP (2004) Influence of wood extractives on moisture sorption and wettability of red oak (*Quercus rubra*), black cherry (*Prunus serotina*), and red pine (*Pinus resinosa*). Wood Fiber Sci 36(4):483–492
30. Hernández RE (2007) Swelling properties of hardwoods as affected by their extraneous substances, wood density, and interlocked grain. Wood Fiber Sci 39(1):146–158
31. Hashemi H, Latibari J (2011) Evaluation and identification of walnut heartwood extractives for protection poplar wood. BioResources 6(1):56–69
32. Mantanis GI, Young RA, Rowell RM (1994) Swelling of wood. Part I: swelling in water. Wood Sci Technol 28(2):119–134
33. Mantanis GI, Young RA, Rowell RM (1995) Swelling of wood. Part III: effect of temperature and extractives on rate of maximum swelling. Holzfor 49(3):239–248
34. Adamopoulos S, Voulgaridis E (2012) Effect of hot-water extractives on water sorption and dimensional changes of black locust wood. Wood Res 57(1):69–78
35. Jankowska A, Drożdżek M, Sarnowski P, Horodeński J (2017) Effect of extractives on the equilibrium moisture content and shrinkage of selected tropical wood species. BioResources 12(1):597–607
36. Takamura N (1968) Studies on hot pressing and drying process in the production of fiber board. III. Softening of fiber components in hot pressing of fiber mat. J J Wood Res Soc 14(2):75–79 **(in Japanese)**
37. Furuta Y, Nakajima K, Nakatani T, Kojiro K, Nakamaru Y (2008) Effects of lignin on the thermal-softening properties of water-swollen wood. J Soc Mater Sci 57:344–349 **(in Japanese)**
38. Furuta Y, Okuyama T, Kojiro K, Miyoshi Y, Kiryu T (2014) Temperature dependence of the dynamic viscoelasticity of bases of Japanese cypress branches and the trunk close to the branches saturated with water. J Wood Sci 60:249–254
39. Matsunaga M, Minato K (1998) Physical and mechanical properties required for violin bow materials II: comparison of the processing properties and durability between Pernambuco and substitutable wood species. J Wood Sci 44:142–146
40. McNaught AD, Wilkinson A (eds) (2014) Compendium of chemical terminology, 2nd edn. Blackwell Scientific Publications, London. https://doi.org/10.1351/goldbook

Publisher's Note